An Artificial Intelligence Method for Predicting the Remaining Useful Life of CNC Milling Machine

Der-Chen Huang[1], Yen-Ting Wu[1], Yen-Hsiang Yang[1], Ying-Yi Chu[2]*

[1] Department of Computer Science and Engineering, National Chung Hsing University, Taiwan
[2] Department of Electronic Engineering, National Kaohsiung Normal University, Taiwan
huangdc@nchu.edu.tw, d110056003@mail.nchu.edu.tw, g108056058@mail.nchu.edu.tw, t4975@mail.nknu.edu.tw

Abstract

For a long time, machining has been an essential technology; it is crucial for shaping a wide range of high-hardness materials. Artificial intelligence (AI) has grown in popularity in recent years owing to advancements in the computing power of hardware, development of AI frameworks in software, and proliferation of data. AI can play a significant role in intelligent production, allowing manufacturers to improve the efficiency of factory information management and effectively reduce production and maintenance costs.

In this study, AI techniques are used to predict the aging trend and determine the remaining useful life (RUL) of milling machine tools for prognostics. The proposed approach helps to mitigate the financial burden associated with accidents caused by the aging of machine tools, achieve intelligent production, and increase production capacity.

Keywords: Intelligent manufacturing, Prognostics, Artificial intelligence (AI), Long short-term memory (LSTM), Support vector regression (SVR)

1 Introduction

Machining is a crucial technology that plays a vital role in our daily lives because it is essential for shaping various products fabricated from high-hardness materials. However, over time, the machinery and equipment used in this process inevitably deteriorate and fail; this can have a direct impact on the reliability, availability, and safety of the final product. If these problems are not addressed promptly, they can result in machinery damage or even accidents involving personnel, as well as loss of processed and raw materials.

The development of machine tools can be traced back to the 15th century, when the manufacturing requirements, particularly for clocks and weapons, led to the creation of threaded lathes and gear-type processing machine tools used by watchmakers. Water-driven cannon boring machines were also used during this period. In the 18th century, the Industrial Revolution accelerated the creation and improvement of various machine tools, including the water-driven cylinder boring machine, which played a role in the development of the steam engine. Subsequently, steam-engine-driven crankshafts became the primary power source for machine tools. In the 19th century, driven by the production of textiles, transportation tools, and arms, a wide range of machine tools emerged, such as the double housing planer, horizontal milling machine, cylindrical grinding machine, gear hobbing machine, and gear shaping machine. Machine tools were initially equipped with electric motors for centralized driving and later developed for single-motor driving. In the early 20th century, various automatic machine tools, profiling machine tools, combined machine tools, and automatic production machines were successively developed, including jig boring machines and thread grinding machines, to improve machining accuracy and meet the requirements of mass production in industries such as automobiles and bearings. During the late 19th century and early 20th century, the lathe gradually evolved into milling machines, planers, grinders, and drillers, laying the foundation for future precision machine tools, production mechanization, and semi-automation. After World War II, in the 1950s, machine tools entered the era of automation with the introduction of numerical control, group control, and automatic production lines. Computerized numerical control (CNC) machine tools emerged as a new type of machine tool that uses computers to control and program processing actions, tool changes, and other functions, by generating control signals based on input instructions.

Traditional methods for detecting faults in CNC machine tools include the observation and automatic diagnosis methods. The observation method relies on human sensory systems to detect various phenomena associated with machine tool failures, such as sparks, abnormal noise, and abnormal heating. By carefully observing the surface of circuit boards with a high failure probability, technicians can determine whether any indication of burning or damage exists, thus narrowing the scope of inspection. By contrast, the automatic diagnosis method utilizes the automatic diagnosis function of the CNC system to collect signals from potentially failed areas and process them using the machine tool's rapid data-processing ability. Diagnostic procedures are then implemented to analyze and determine whether or not a system failure occurs. However, regular maintenance checks on these methods are required to ensure the optimal condition of the machine, regardless of

*Corresponding Author: Ying-Yi Chu; Email: t4975@mail.nknu.edu.tw
DOI: https://doi.org/10.70003/160792642026012701007

the presence of any current faults. Consequently, the cost of regular maintenance, including labor and time, for CNC machine tools is considerably high. However, with the continuous advancement of technology and the emergence of Industry 4.0, numerous factories are now striving to systematically and efficiently maintain or even enhance the production capacity of their production lines through information digitization. They are aiming to leverage computers in decision-making processes and achieve intelligent production. In contrast to traditional scheduled maintenance, the novel approach of predictive maintenance enables maintenance actions to be performed only when they are required. This approach significantly reduces the expenses associated with the operation of machine tools.

In recent years, artificial intelligence (AI) has grown in popularity owing to the advancements in computer hardware technology, development of user-friendly software frameworks, and exponential growth of big data. Thus, the aim of this study is to utilize AI to implement a fundamental prognostics method in intelligent production. Specifically, the method involves learning and predicting the future evolution progress of a physically aging system of tools.

The paper is structured into five sections. Section 1 introduces the motivation and purpose of the study. Section 2 presents the relevant background knowledge and related studies. Section 3 provides a detailed description of the method for estimating the remaining useful life (RUL) of CNC milling machine tools. Section 4 presents the experimental results. Finally, Section 5 concludes the paper.

2 Relevant Research Background and Methods

2.1 Overview of Machining and Intelligent Manufacturing

Machining is a manufacturing process that involves altering the shape and dimensions of a workpiece using machine tools or processing machines. This process can be categorized into cold and hot machining, depending on the temperature at which the workpiece is processed. Cold machining is characterized by processing at room temperature, thereby avoiding any chemical or physical reactions in the workpiece. Examples of cold machining include pressure processing and cutting processing. By contrast, hot machining involves processing the workpiece at high temperatures, thus increasing the likelihood of chemical or physical reactions occurring. Examples of hot machining include heat treatment, welding, and forging. This type of machining, which involves removing excess material, is also referred to as subtractive manufacturing.

In the process of cutting, tool condition monitoring (TCM) plays a crucial role in monitoring a tool's performance and ensuring the desired surface finish of the workpiece [1]. The deterioration of the tool during cutting can have direct implications on the reliability, availability, and safety of the final product, resulting in lower quality and a rougher surface of the workpiece. Failure to detect tool deterioration in real time can result in machine damage, accidents involving personnel, and loss of processed materials and raw materials. To avoid such risks, an effective monitoring system should be implemented, with prognostics and health management (PHM) being one of the methods used [2-4].

According to the onset of the 4th industrial revolution, the digital transformation with AI technology has led to tremendous developments. PHM technology plays a crucial role in assessing and predicting system degradation [5]. Furthermore, due to the continuous evolution of hardware computational capabilities and deep learning models, RUL prediction relies on tracking the health status of the system. Therefore, its accuracy and efficiency have significantly enhanced. To avoid irreversible losses caused by accidental failure, the reliability and safety of the PHM methods are validated in numerous research works [6-7].

The PHM process mainly consists of the following steps: data acquisition, data processing, condition assessment, diagnosis, prognostics, and decision-making assistance. Condition assessment and prognostics can be employed to continuously assess and predict the tool wear. The purpose of prognostics [8-9] is to estimate the RUL of components, sub-systems, and the system [10]; thus, prognostics can be applied in TCM to estimate the RUL. Figure 1 shows the RUL, where the x-axis represents the system runtime and y-axis represents the system efficiency. The full line represents the historical system efficiency, whereas the dashed line represents the actual future trend of the system efficiency. The system efficiency decreases over time until it fails at a certain point. The dashed line indicates the RUL before failure.

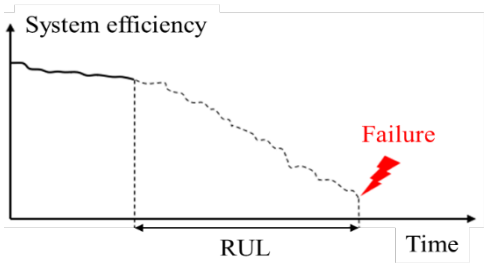

Figure 1. Schematic diagram of RUL

As shown in Figure 2, prognostics can be approached through three different methods: model-based, data-driven, and hybrid. The model-based method [11-12] involves developing a mathematical model that represents the physical behavior of the system, including the aging process. This derived model can then be used to simulate the system's future evolution, allowing for the observation of aging trends and estimation of RUL. The main advantage of this method is its high accuracy, because the mathematical model directly reflects the system's actual performance. However, it is limited in its applicability to specific situations and is not applicable to most situations; it can also be challenging and expensive to implement in practical operations. The data-driven method [13] relies on data collected from sensors, which are processed and transformed into a health index (HI) that represents the state of the system

and allows for the estimation of future aging trends. This method offers high applicability, low operational costs, and ease of implementation. However, it is not as accurate as the model-based method. The hybrid method combines elements of both the model-based and data-driven methods, depending on the specific requirements of the situation. A comparison between the model-based and data-driven methods is presented in Table 1, and the data-driven method is adopted in this study.

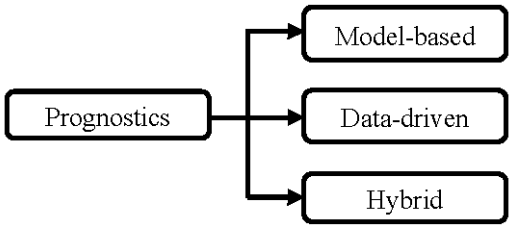

Figure 2. Prognostics methods

Table 1. Comparison between prognostics methods

	Model-based	Data-driven
Applicability	low	**high**
Accuracy	**high**	low
Cost of practical operation	high	**low**
Practical operation complexity	high	**low**

2.2 Introduction to Dataset

The dataset used in this study is from the 2010 PHM Society Conference Data Challenge [14]; it is suitable for estimating the RUL of CNC milling machine tools. The data for force, vibration, and acoustic emission (AE)-root mean square (RMS) are collected using a dynamometer, an accelerometer, and an acoustic emission sensor, respectively. Six tools, namely, c1, c2, c3, c4, c5, and c6, are used, and each tool begins collecting data when it is completely new. Data from 315 machining cycles are used, where c1, c4, and c6 are used to train the model and c2, c3, and c5 are used to test the training effect.

2.2.1 Operating Conditions

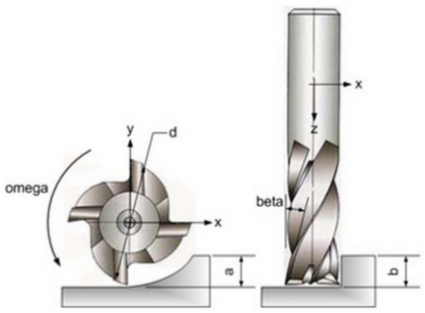

Figure 3. Y depth of cut (left) and X depth of cut (right)

Some of the parameters set during machining can be used to describe the machine operating conditions when running. The spindle speed is 10400 RPM, feed rate is 1555 mm/min, Y depth of cut (radial) is 0.125 mm, Z depth of cut (axial) is 0.2 mm, and sample rate is 50k Hz. The horizontal and vertical depths of cut are shown in Figure 3. These parameters include the material, type, and cutting path of the tool and the object to be machined, all of which affect the final data collection results. This dataset is collected from the six tools in the same environment.

2.2.2 Data Collection

Data for force, vibration, and AE-RMS are acquired by using a dynamometer, an accelerometer, and an acoustic emission sensor, respectively. The signals of force and vibration can be further subdivided into x-, y-, and z-axis directions. Each tool is completely new before use, and 315 machining cycles are implemented.

2.2.3 Equipment Setup

The equipment used in this dataset is listed in Table 2. A Röders Tech RFM 760 high-speed CNC machine is used, and the material to be machined is stainless steel HRC52. As shown in Figure 4, the tool is a 2-flute ball nose cutter, where 2-flute indicates that this tool has two blades and ball nose indicates that the cutter head is rounded. The three sensors used are all from Kistler. The dynamometer is mounted between the machining table and the object to be machined, and the accelerometer and acoustic emission sensor are mounted on the object to be machined.

Table 2. Table of equipment used for the dataset

Equipment name	Related specifications
High-speed CNC machine	Röders Tech RFM 760
Material to be machined	stainless steel (HRC52)
Tool	2-flute ball nose cutter
Dynamometer	Kistler quartz 3-component platform dynamometer
Accelerometer	Kistler piezo
Acoustic emission sensor	Kistler acoustic emission (AE) sensor
Data collection adapter	NI DAQ PCI 1200 board with 12KHz

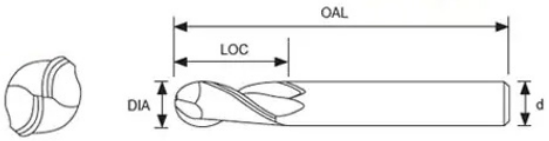

Figure 4. Tool appearance

3 Research Method

In this study, the experimental results of German sensor companies are utilized, a graphical method is employed to analyze the raw data, the HI is determined by using graphical features, and different models and a sliding window are used to estimate the future aging trend of the tool. Finally, the RUL of the tool is calculated.

The flow structure of the research method is shown in Figure 5. First, the data are pre-processed. Then, feature acquisition is performed based on the original data collected, followed by data fusion using the collected data.

The corresponding force diagrams are created based on the fusion results of each machining cycle, followed by the identification of convex hull for each machining cycle. Finally, the appropriate shape features of the convex hull are obtained based on each force diagram; these features represent the tool's health status, that is, the HI. Obtained through a series of pre-processing steps, the HI is fed into the trained regression prediction model for aging trend projection, and then, the RUL is calculated using the derived aging system evolution process.

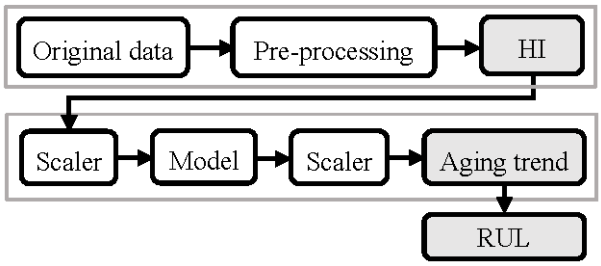

Figure 5. Flow structure of the research method

3.1 Data Pre-Processing

The prognostics method, whether model-based or data-driven, requires first determining the HI that represents the system state, and then using regression method to predict the future trend. Therefore, the main goal of pre-processing data is to run a series of processes on the raw data to obtain a HI that effectively represents the state of the system. The data pre-processing of this study is shown in Figure 6. First, the features are acquired from the collected raw data, then the data are fused and the force diagrams are generated based on each machining cycle. The force diagrams are then used to find the convex hull. Finally, according to the convex hull of the force diagrams, the appropriate shape features are identified, which represent the health status of the tool.

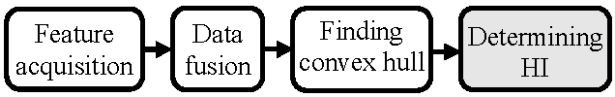

Figure 6. Flowchart of data pre-processing

3.1.1 Feature Acquisition

Feature acquisition refers to the results of a force visualization experiment conducted by Pro-micron [15], a German sensor company, as shown in Figure 7. The bottom part of the image shows three different tool conditions: new, worn, and broken, from left to right. The top of the image is the corresponding force diagram, with the x and y axes representing the horizontal forces in the x and y directions, respectively. The size of the force diagram formed by the new tool is relatively small compared with those by the other two, indicating that the sharpness of the tool surface is sufficiently high; therefore, the force required during the machining process is smaller. When the tool starts to wear gradually, the force diagram becomes larger, which indicates that the tool gradually wears, resulting in the decline in the sharpness of the tool surface and increasing the force required during the machining process. A significant change can be observed in the force diagram when the tool breaks. Therefore, the experimental force visualization result can be used to estimate that the tool's x and y forces gradually increase with the hours of use until failure behavior occurs. As a result, in terms of feature acquisition, the x and y forces are obtained as features for the prediction of the aging trend.

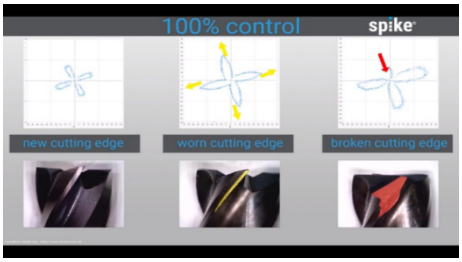

Figure 7. Experimental results of force pro-micron spike®

3.1.2 Data Fusion

As shown in Figure 8, after the x and y forces are extracted, each corresponding x and y force is combined into a (x, y) coordinate point. As the data are collected at a rate of 50 kHz, several x and y force data are present in each machining cycle; thus, the x and y forces of each machining cycle can form a 2D force diagram of that machining cycle, where x and y axes are the forces in the x and y directions, respectively.

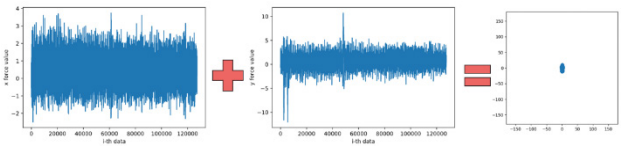

Figure 8. Data fusion diagram for the first machining cycle of the c1 tool

3.1.3 Finding Convex Hull

After the complex 2D force diagram was obtained for each machining cycle, it needed to be simplified and the aging trend of the tool predicted; the results of Pro-micron force visualization experiment indicated that the force would continue to increase with the increase of hours of use, that is, the convex hull of the 2D force diagram would become larger. Therefore, as shown in Figure 9, the Graham Scan [16] algorithm is used to find the convex hull part, that is, the convex hull that can cover all coordinate points in the force diagram.

As shown in Figure 10, the first step is to find the coordinate point with the smallest y-value as the starting point, S, in a plane full of coordinate points. If several coordinate points with the smallest y-value exist, the one with the smallest x-value (the leftmost one) is considered.

In the second step, as shown in Figure 11, the remaining coordinate points are sorted according to the polar angle, where the polar angle is the polar coordinate angle formed by the line segment between the point and starting point (S), beginning from the right side and visiting counterclockwise.

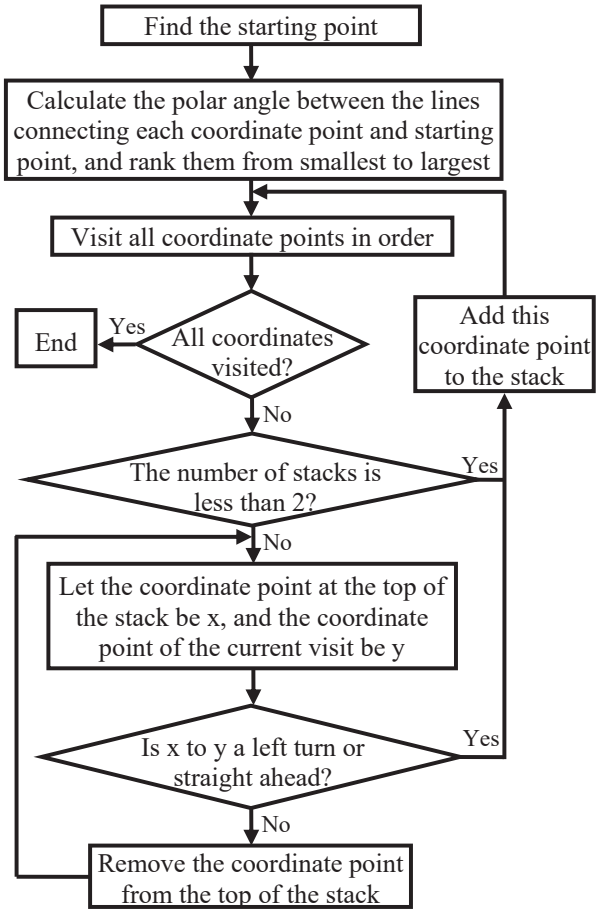

Figure 9. Graham Scan flowchart

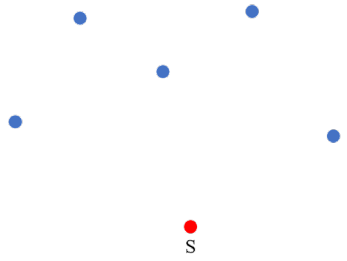

Figure 10. Finding the starting point in Graham Scan

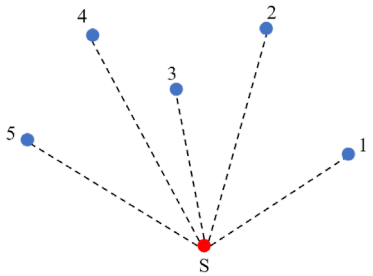

Figure 11. Determining the order of visits in Graham Scan

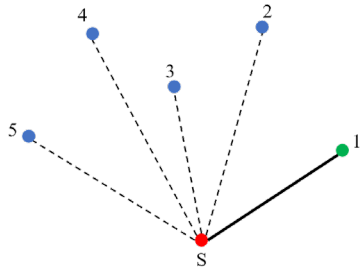

Figure 12. Visiting coordinate point 1 in Graham Scan

In the third step, a stack must be established to store all the current convex hull coordinates, and these coordinates must then visited and added to the stack in the order of the second step. If the direction of movement is to the left, then the coordinates are added to the stack. If the direction of movement is to the right, the coordinates at the top of the stack are removed until all coordinates have been visited. See the following example for further explanation. As shown in Figure 12, the first visit is to coordinate point 1, which is added to the stack directly because no record of the previous direction of movement is present.

As shown in Figure 13, coordinate point 2 is visited and compared with the previous direction of movement, which is to the left; thus, this coordinate point is added to the stack.

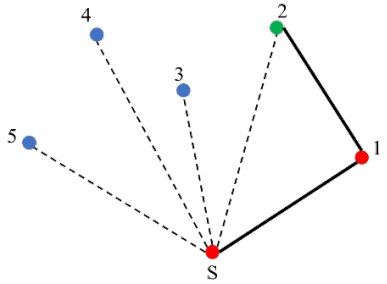

Figure 13. Visiting coordinate point 2 in Graham Scan

As shown in Figure 14, coordinate point 3 is visited and compared with the previous direction of movement, which is to the left; thus, this coordinate point is added to the stack.

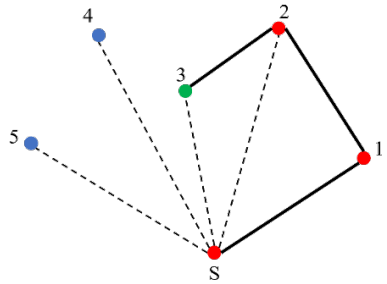

Figure 14. Visiting coordinate point 3 in Graham Scan

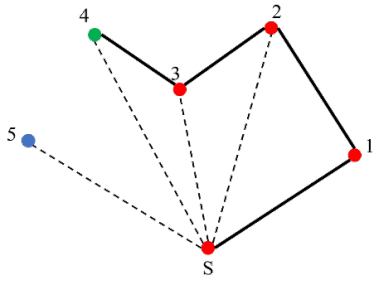

Figure 15. Visiting coordinate point 4 in Graham Scan (before adjustment)

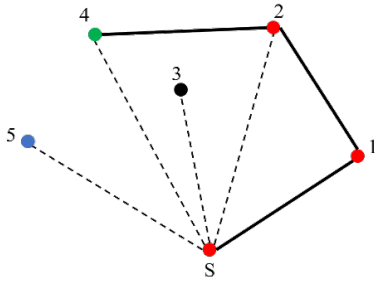

Figure 16. Visiting coordinate point 4 in Graham Scan (after adjustment)

As shown in Figure 15, coordinate point 4 is visited and compared with the previous direction of movement, which is to the right; thus, coordinate point 3 should be removed from the stack. If coordinate point 2 is linked to coordinate point 4, coordinate point 3 will be included in the area of the convex pull polygon. Subsequently, the direction of movement from coordinate point 2 to coordinate point 4 will be determined. If it is still to the right, then coordinate point 2 should be removed from the stack, and so on. In this case, the direction of movement from coordinate point 2 to coordinate point 4 is to the left; therefore, coordinate point 4 is added to the stack. The result of the visit up to coordinate point 4 is shown in Figure 16.

As shown in Figure 17, coordinate point 5 is visited and compared with the previous direction of movement, which is to the left; thus, this coordinate point is added to the stack. All coordinate points are now visited, and the whole process is completed.

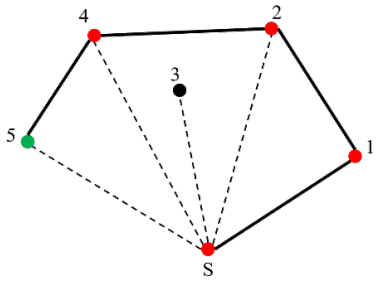

Figure 17. Visiting coordinate point 5 in Graham Scan

As shown in Figure 18, the 2D force diagram convex hull of the c1 tool in the dataset changes at different time points in the 1st machining cycle (brand new), 150th machining cycle (gradual wear), and 315th machining cycle (later period), and a trend of gradual increase in the size of its convex hull shape can be observed.

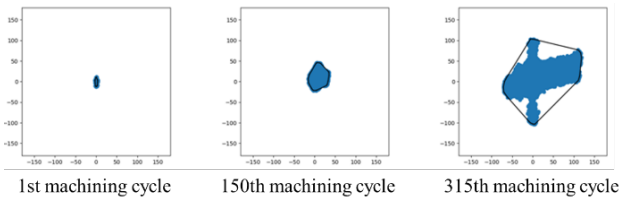

Figure 18. Changes in the force diagram of the convex hull for different machining cycles of the c1 tool

3.1.4 Determining HI

As the hours of using the tools increases, the amount of change in the convex hull of the force diagram varies; thus, it can represent the health condition of the tool. In this study, the following five shape characteristics of the convex hull are considered as candidates for the HI: the longest distance of the convex hull, amount of change in the longest distance from the previous convex hull, area of the convex hull, amount of change from the area of the previous convex hull, and sum of the changes in the maximum distance and area of the convex hull; the most suitable one among these is selected as the HI. Based on all the tools in the 2010 PHM Society Conference Data Challenge dataset, that is, tools c1 to c6, the analysis graphics of different shape features of the convex hull during the machining cycle are shown in Figure 19 to Figure 24; the x-axis represents the machining cycle, the y-axis represents the value of the feature using this graphic, and Δ represents the amount of change from the previous machining cycle time point.

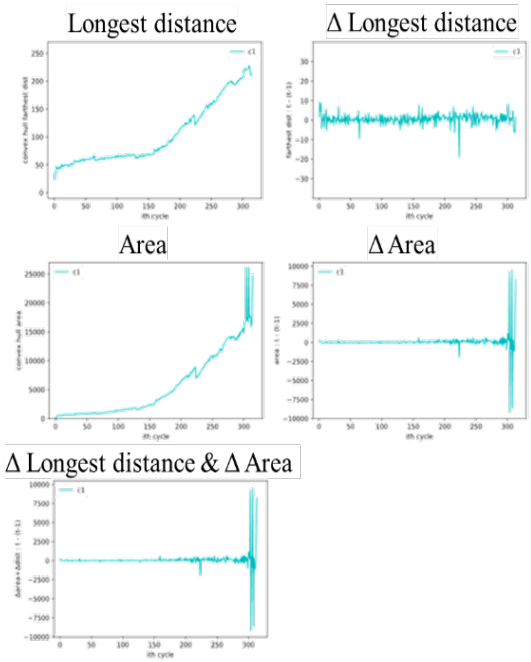

Figure 19. Changes in convex hull characteristics of the force diagram for all machining cycles of the c1 tool

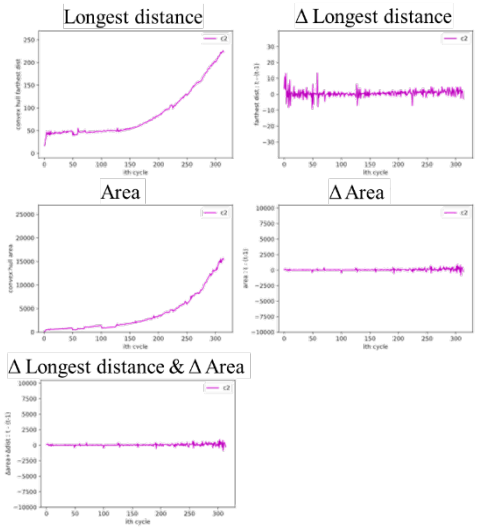

Figure 20. Changes in convex hull characteristics of the force diagram for all machining cycles of the c2 tool

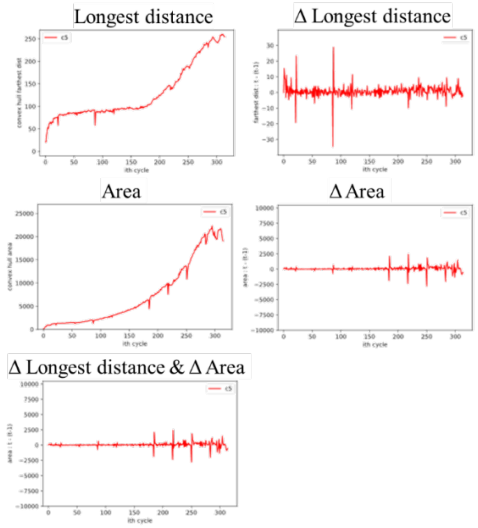

Figure 23. Changes in convex hull characteristics of the force diagram for all machining cycles of the c5 tool

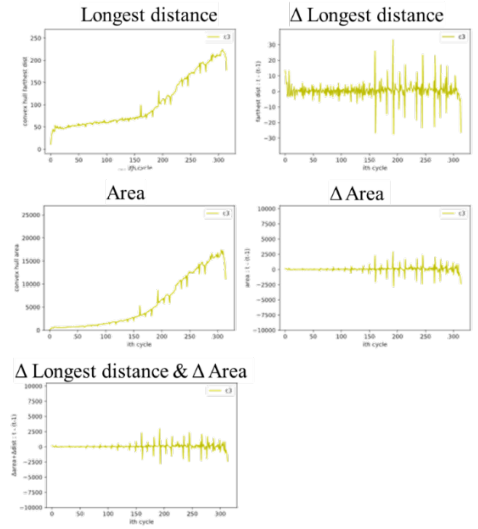

Figure 21. Changes in convex hull characteristics of the force diagram for all machining cycles of the c3 tool

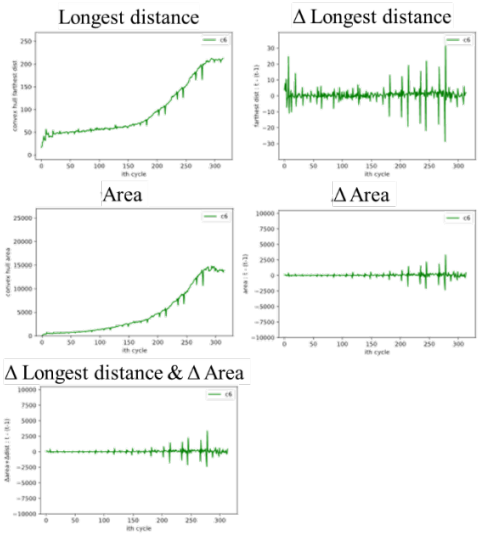

Figure 24. Changes in convex hull characteristics of the force diagram for all machining cycles of the c6 tool

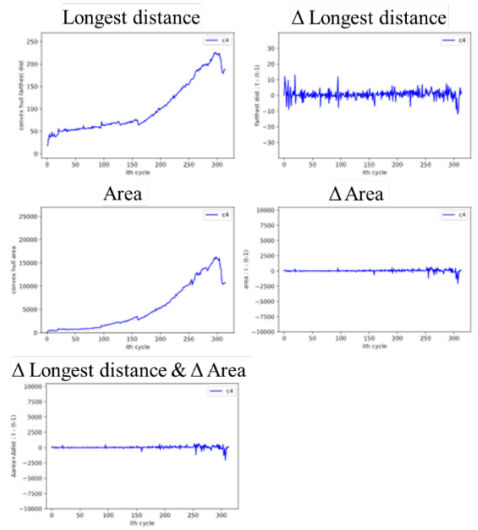

Figure 22. Changes in convex hull characteristics of the force diagram for all machining cycles of the c4 tool

These results reveal that the longest distance of the convex hull and the area of the convex hull clearly increase with increasing hours of use, which is more in line with the HI of this study than other characteristics. Based on this characteristic, the tool is assumed to be completely new at the beginning with the lowest characteristic value, and as the tool ages with increased hours of use, the characteristic value gradually increases until a potential failure behavior occurs; therefore, the final selection is made from the longest distance of the convex hull and the area of the convex hull. In this study, the first predicted time (FPT) represents the time point when significant decline begins to occur, as shown in Equation (1), where $x(t_j)$ represents the RMS value at time point t_j , u is the mean value of RMS from the beginning to time point t_j , and σ is the standard deviation of RMS values from the beginning to time point t_j . The concept behind this method is to determine whether or not it is the extreme value. Most of the data from a normal distribution are concentrated in the range

of 1–2 times the standard deviation from the mean value, with a few exceptions concentrated in 3 times the standard deviation. Three times the standard deviation indicates that the value is an extreme value, implying that abnormalities may occur for the tool at that time point, causing the value at that time point to be more different from the previous value. Therefore, this method can be used to find the time point at which a significant decline begins to occur. In addition, from the time point where the condition is met, five consecutive time points must meet the condition before the time point is considered to be the starting point of significant decline we are searching.

Figure 25 to Figure 30 show the comparison results of the longest distance of each tool using the convex hull of the force diagram and the calculation of the FPT of the convex hull area.

$$\left|x\left(t_j\right)-u\right| \geq 3\sigma, t=i, i+1, \ldots, i+v-1 \quad (1)$$

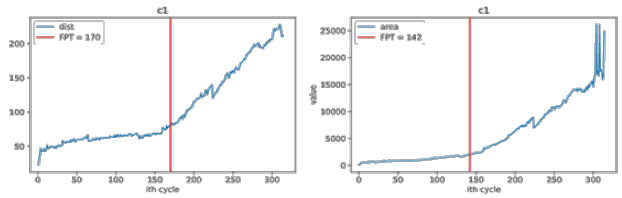

Figure 25. Comparison of the c1 tool's longest distance (left) and area (right) FPT

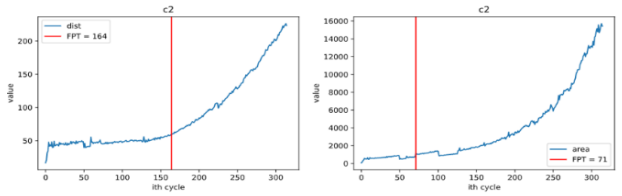

Figure 26. Comparison of the c2 tool's longest distance (left) and area (right) FPT

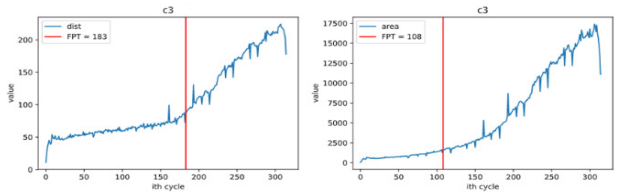

Figure 27. Comparison of the c3 tool's longest distance (left) and area (right) FPT

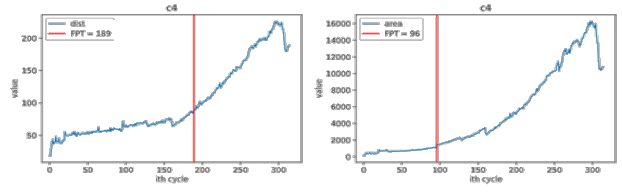

Figure 28. Comparison of the c4 tool's longest distance (left) and area (right) FPT

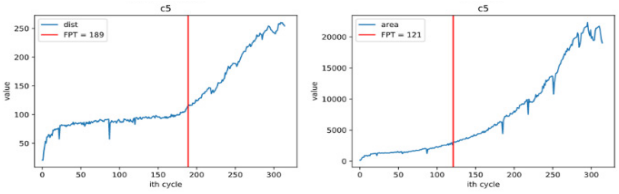

Figure 29. Comparison of the c5 tool's longest distance (left) and area (right) FPT

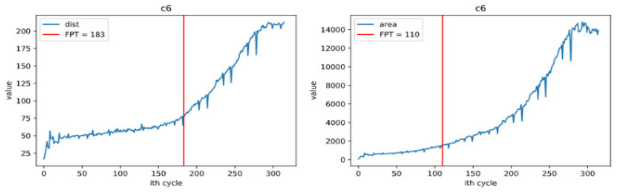

Figure 30. Comparison of the c6 tool's longest distance (left) and area (right) FPT

A combination of these results reveals that the FPT of the convex hull area is reached earlier than the convex hull longest distance, that is, the convex hull area reflects the aging phenomenon earlier than the longest distance of the convex hull; thus, the convex hull area is finally selected as the HI to reflect to the tool aging condition.

3.1.5 Data Pruning and Threshold Setting

Tools fail as the hours of use increase. To predict the aging trend of tools, this study only collects data before the failure behavior occurs and sets a threshold value based on the degree of wear to stop using the tool. Figure 31 shows the comparison before and after data pruning and threshold value setting. The end part of the c1 tool (cyan line) clearly shows oscillation, which is an abnormal phenomenon that can lead to a potential failure behavior and must be removed. Subsequently, for the last degree of wear, all tools are examined and the threshold value is set at the corresponding position; the threshold value will vary depending on the decision.

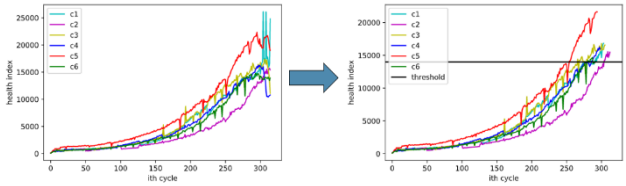

Figure 31. Comparison before and after data pruning and threshold setting

3.2 Aging Trend Projection and RUL Estimation

The sliding window method is used to project the trend of aging. As shown in Equation (2), where input end x and output end y are HIs, t represents the present time, n represents the length of time, and f represents the trained regression prediction model, the health pointers for the present and previous n time units are fed into the trained regression prediction model and the model outputs the HI for the next time point. The new HI is then considered as inputs, and the oldest input is replaced to form new input, which is fed into the model again to obtain the HI for the

next time point. This process is repeated again and again to form a sequence diagram of the HI related to each time point, which can be used to project the future aging trend of the tool at that time point.

$$f\left(\left[x_{t-(n-1)},\ldots,x_t\right]\right)=y_{t+1} \tag{2}$$

Figure 32 displays the c3 tool in the dataset. The left graph shows the aging trend projection, where the x-axis represents the machining cycle and y-axis represents the HI or tool wear. The right graph depicts RUL estimation, where the x-axis represents the machining cycle and y-axis represents the RUL at that time point. Based on the assumption that the present time is at the 50th machining cycle, the sliding window method is used to project the future aging trend (shown as the red line) and the actual future trend (shown as the black dashed line). The actual RUL is the time when the black dashed line reaches the threshold value from the 50th machining cycle, whereas the estimated RUL is the time when the red line reaches the threshold value from the 50th machining cycle. For the graph on the right, the black dashed line indicates the actual RUL and the red solid line indicates the estimated RUL. The estimated RUL is higher than the actual RUL at the 50th machining cycle. In addition, the tool wear level does not increase significantly at the beginning, resulting in an inaccurate RUL prediction. After the tool is used for a certain period and the wear level starts to increase, the RUL prediction accuracy increases.

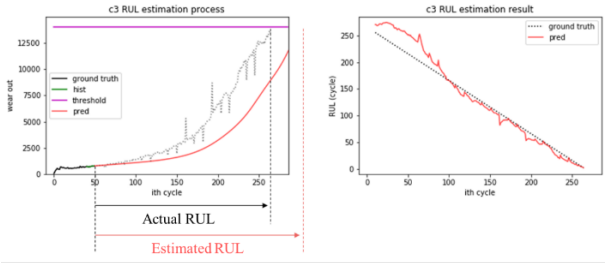

Figure 32. Aging trend projection and RUL estimation graph

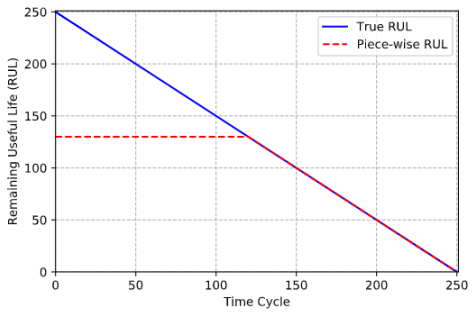

Figure 33. Schematic diagram of piece-wise RUL

As the initial RUL prediction is not sufficiently accurate, the piece-wise RUL [17-18] method is used in the effectiveness evaluation in this study. When an initial error occurs to the system at a certain time point, that is, when the HI starts to change significantly, the RUL decreases with the hours of use and no indication exists prior to the initial error; thus, the predicted result is not very satisfactory. As shown in Figure 33, the x-axis represents the time and y-axis represents the RUL at that point of time. The actual RUL is represented by the solid blue line, which decreases linearly with the hour of use, step by step, towards the time point of failure.

3.3 Performance Indicators

The first is accuracy [19], which shows the average accuracy of the RUL prediction. The value closer to 1 indicates higher accuracy, while a value further from 1 indicates poorer accuracy. Equation (3) shows that T represents total time and t represents each processing cycle time point. Equation (3) sums and averages the negative power of the exponential for each time point, where x represents the proportion of the estimated error that is accounted for by the actual. A value of 1 indicates agreement between the estimated and actual values, when the error is 0; while a larger error value yields a smaller value.

$$Accuracy=\frac{1}{T}\sum_{t=1}^{T}e^{-\left|\frac{RUL_{real}(t)-RUL(t)}{RUL_{real}}\right|} \tag{3}$$

The second is precision [19], which represents the average accuracy of the prediction. A lower value indicates better concentration, while a higher value indicates less concentration. This is calculated using Equation (4), where T represents the total time and t represents each processing cycle time point. ε represents the predicted error, as shown in Equation (5), and $\bar{\varepsilon}$ represents the average value of the error, as shown in Equation (6).

$$Precision=\sqrt{\frac{\sum_{t=1}^{T}\left(\varepsilon(t)-\bar{\varepsilon}\right)^2}{T}} \tag{4}$$

$$\varepsilon(t)=RUL_{real}(t)-RUL(t) \tag{5}$$

$$\bar{\varepsilon}=\frac{1}{T}\sum_{t=1}^{T}\varepsilon \tag{6}$$

The third is mean absolute percentage error (MAPER) [19], which represents the percentage of the prediction average error. A lower MAPER value is better, as shown in Equation (7), where ε represents the predicted error. As shown in Equation (5), all time points calculated in Equation (7) are summed and averaged. The proportion of predicted errors on the actual at each time point is calculated, followed by multiplying by 100 into percentage and considering the absolute value.

$$MAPER=\frac{1}{T}\sum_{t=1}^{T}\left|\frac{100\cdot\varepsilon(t)}{RUL_{real(t)}}\right| \tag{7}$$

The fourth is runtime, which indicates the running time. A lower runtime is better, as shown in Equation (8), where C represents the time spent to project the aging trend. This equation is applied to calculate the total sum of the time spent on projecting the aging trend at all time points.

$$Runtime = \sum_{t=1}^{T} C(t) \tag{8}$$

3.4 Data Acquisition and Prognostics

To predict the aging trend of CNC milling machine tools, there are three key stages required to process the data collection. As illustrated in Figure 34, the first phase is to collect data from a CNC milling machine. It is important to ensure the data collected is effective and trustworthy, therefore the qualified data can be analyzed with AI techniques. The next stage is storage, the valid data is stored in a permanent cloud drive. When the data is properly stored, it can be readily accessed for prognostics when needed. After all of the data is stored, AI models are used to predict the aging trend and determine the RUL of milling machine tools.

Figure 34. A data acquisition and prognostics system

4 Experimental Results and Discussion

4.1 Model Evaluation for RUL Prediction Results with Different Tools

The experimental results are shown in Table 3. Different models were used to predict the RUL for different tools in the test set, and the data for 10 times were recorded and then averaged as the average performance of each model; the bold text in the table represents the best performance pointer among the three models.

Table 3. Evaluation of the effectiveness of RUL prediction results for the dataset

Model	Metrics	c2	c3	c5
ANN	Accuracy	0.8618	0.8996	0.8985
	Precision	10.36	8.15	6.8
	MAPER	19.77	12.76	12.88
	Runtime (s)	1020.17	831.66	758.84
SVR	Accuracy	**0.9564**	0.942	0.8958
	Precision	**4.46**	**4.05**	8.43
	MAPER	**4.79**	12.18	13.65
	Runtime (s)	**6.08**	**4.89**	**4.46**
LSTM	Accuracy	0.9205	**0.9491**	**0.9446**
	Precision	5.41	4.19	**4.86**
	MAPER	9.54	**5.78**	**6.62**
	Runtime (s)	1002.98	833.04	753.44

The aforementioned findings show that both support vector regression (SVR) and long short-term memory (LSTM) exhibit satisfactory overall performance. SVR demonstrates comparable accuracy to LSTM, but with a concentrated precision and a more stable performance. On the contrary, LSTM generally achieves the highest accuracy of the three models, with accuracy levels similar to SVR. In terms of overall performance LSTM slightly outperforms SVR when runtime is disregarded. However, when considering runtime, SVR is significantly faster while maintaining comparable performance to LSTM. This discrepancy in runtime can be attributed to the complexity of the models. In contrast to LSTM, which incorporates a greater number of neurons and gates (i.e., input gate, forget gate, output gate), SVR exhibits a more direct and rapid data transfer process. Consequently, SVR is preferred in practical applications that require real-time capabilities. Conversely, if real-time constraints are not a concern, LSTM remains a viable option.

4.2 Testing the Applicability of the Prediction Model Using Simulation Data

The flowchart of the simulation data generation in this study is shown in Figure 35. First, the parameters are initialized for the predetermined machining conditions, followed by listing all possible cases of tooth breakage. If the tool has n blades, then all possible cases of tooth breakage are $C_1^n - C_n^n$. Therefore, the life cycle is generated based on the various cases of tooth breakage. First, the parameters are set with ±10% as the upper limit. Then, the starting and ending amounts of increase in the life cycle rose diagram and the total processing cycle are set. For each processing cycle, the aging curve set in the initialization is used to calculate the length of the current process rose diagram, and the current-processing-cycle rose diagram is generated by using the rose diagram formula.

The initialization of the parameters is presented in Table 4. Based on the preliminary analysis, several parameters that can be set are listed and adjusted appropriately based on the assumed machining conditions. In Figure 36, the left figure shows the rose diagram at the first machining cycle, with a length (center of the circle to the vertex of the petal) of 20±10%. The middle figure shows the rose diagram at the last processing cycle, with a length of 20±10%+100±10%. The right figure is the last rose diagram with tooth breakage, where only one tooth breaks, and the broken tooth is in the upper right. According to the number of blades set in this case, $C_1^4 - C_4^4$ cases of tooth breakage exist; thus, the life cycle is generated based on each case. A signal-noise-ratio setting is added to make the rose diagram more realistic rather than the ideal perfectly smooth curve. As shown in Figure 37 for the aging curve, the x-axis represents the processing cycle ratio (0–1) and the y-axis represents the ratio of the amount of increase in the rose diagram length (0–1). The current processing cycle is calculated as per the aging curve function after first dividing it by the total processing cycle and converting it to a process ratio of 0–1. As shown in Equation (9), the polar coordinate rose diagram formula is used to draw the

rose diagram of that processing cycle, where *l* is the length, that is, the length from the center of the circle to the vertex of the petal, and n represents the petal number parameter. If *n* is an even number, the rose diagram has 2*n* petals, and if *n* is an odd number, the rose diagram will have *n* petals.

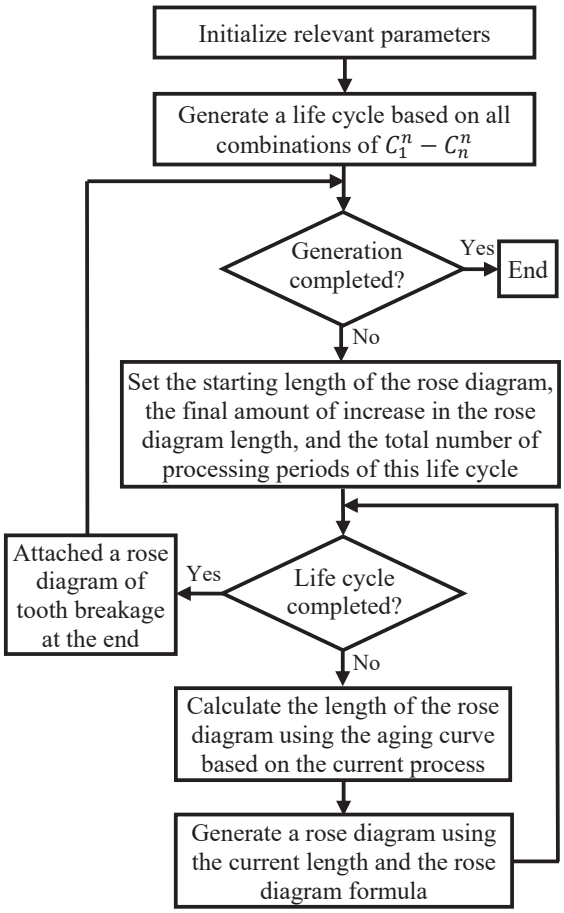

Figure 35. Flowchart of simulation data generation

Table 4. Simulation data parameter settings

Parameter name	Value
Number of blades (number of teeth)	4
Average processing cycle	100
Initial length of rose diagram	20
Final amount of increase of rose diagram	100
Processing cycle sampling volume	1000
Signal-noise-ratio	0.1
Aging curve	$y = e^{4(x-1)}$

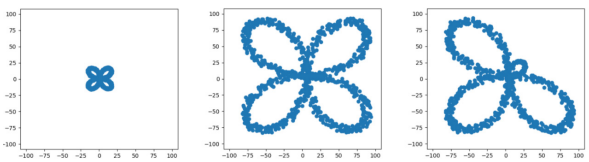

Figure 36. Variation in force diagram of simulation data

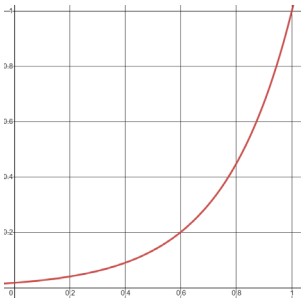

Figure 37. $y = e^{4(x-1)}$ aging curve

$$r = 1 \times \sin(n \times \theta) \tag{9}$$

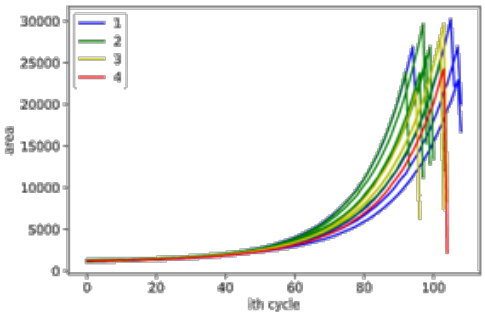

Figure 38. Simulation data life cycle

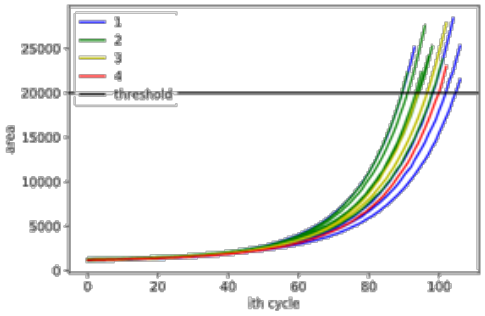

Figure 39. Simulation data life cycle after pruning and threshold setting

The convex hull area is used as the HI to observe the aging trend after generating all the life cycles of the broken tooth cases of $C_1^n - C_n^n$, as shown in Figure 38. The blue line represents the cases with only one broken tooth, green line represents the cases with two broken teeth, yellow line represents the cases with three broken teeth, and red line represents the cases with all teeth are broken. As depicted in Figure 39, only information before the failure behavior is acquired and the appropriate threshold value is set based on the available information.

Based on the practice of the 2010 PHM Society Conference Data Challenge, 50% of the aging trend in the middle is used as the training set and the remaining 50% as the test set; LSTM is employed as the regression prediction model. Figure 40 shows the RUL prediction results for various tooth breakage cases in the test set.

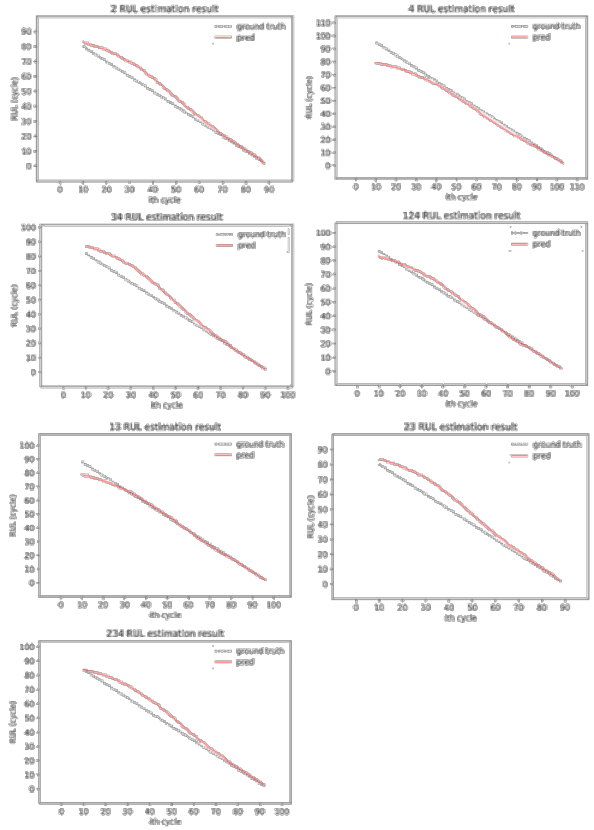

Figure 40. RUL prediction results for the test set

5 Conclusion

The aim of this study is to estimate the RUL of milling tools using publicly available datasets. First, the preprocessing of the raw data involves feature extraction, data fusion, and convex-hull finding to obtain the HI for predicting the aging trend. The sliding window method is then used to feed the HI, which has temporal correlation, into a trained regression prediction model to predict the tool's aging trend and calculate its RUL.

Furthermore, three different models, namely, artificial neural network (ANN), SVR, and LSTM are compared. Based on the experimental results, SVR is recommended in the online environment for real-time applications owing to its low runtime and comparable performance. By contrast, LSTM is suitable for offline applications where time constraints are not a concern.

References

[1] B. Sick, On-Line and Indirect Tool Wear Monitoring in Turning with Artificial Neural Networks: a Review of More than a Decade of Research, *Mechanical Systems and Signal Processing*, Vol. 16, No. 4, pp. 487-546, July, 2002. https://doi.org/10.1006/mssp.2001.1460

[2] A. Heng, S. Zhang, A. C. C. Tan, J. Mathew, Rotating machinery prognostics: State of the art, challenges and opportunities, *Mechanical Systems and Signal Processing*, Vol. 23, No. 3, pp. 724-739, April, 2009. https://doi.org/10.1016/j.ymssp.2008.06.009

[3] K. Medjaher, D. A. Tobon-Mejia, N. Zerhouni, Remaining Useful Life Estimation of Critical Components With Application to Bearings, *IEEE Transactions on Reliability*, Vol. 61, No. 2, pp. 292-302, June, 2012. https://doi.org/10.1109/TR.2012.2194175

[4] J. Z. Sikorska, M. Hodkiewicz, L. Ma, Prognostic modelling options for remaining useful life estimation by industry, *Mechanical Systems and Signal Processing*, Vol. 25, No. 5, pp. 1803-1836, July, 2011. https://doi.org/10.1016/j.ymssp.2010.11.018

[5] A. A. Adekunle, I. Fofana, P. Picher, E. M. Rodriguez-Celis, O. H. Arroyo-Fernandez, Analyzing Transformer Insulation Paper Prognostics and Health Management: A Modeling Framework Perspective, *IEEE Access*, Vol. 12, pp. 58349-58377, April, 2024. https://doi.org/10.1109/ACCESS.2024.3391823

[6] E. Zio, Prognostics and Health Management Methods for Reliability Prediction and Predictive Maintenance, *IEEE Transactions on Reliability*, Vol. 73, No. 1, pp. 41-41, March, 2024. https://doi.org/10.1109/TR.2024.3356816

[7] Y. Hu, X. Miao, Y. Si, E. Pan, E. Zio, Prognostics and health management: A review from the perspectives of design, development and decision, *Reliability Engineering & System Safety*, Vol. 217, Article No. 108063, January, 2022. https://doi.org/10.1016/j.ress.2021.108063

[8] A. K. S. Jardine, D. Lin, D. Banjevic, A review on machinery diagnostics and prognostics implementing condition-based maintenance, *Mechanical Systems and Signal Processing*, Vol. 20, No. 7, pp. 1483-1510, October, 2006. https://doi.org/10.1016/j.ymssp.2005.09.012

[9] D. A. Tobon-Mejia, K. Medjaher, N. Zerhouni, CNC machine tool's wear diagnostic and prognostic by using dynamic Bayesian networks, *Mechanical Systems and Signal Processing*, Vol. 28, pp. 167-182, April, 2012. https://doi.org/10.1016/j.ymssp.2011.10.018

[10] X. Kong, J. Yang, Remaining Useful Life Prediction of Rolling Bearings Based on RMS-MAVE and Dynamic Exponential Regression Model, *IEEE Access*, Vol. 7, pp. 169705-169714, November, 2019. https://doi.org/10.1109/ACCESS.2019.2954915

[11] D. Chelidze, J. P. Cusumano, A Dynamical Systems Approach to Failure Prognosis, *Journal of Vibration and Acoustics*, Vol. 126, No. 1, pp. 2-8, January, 2004. https://doi.org/10.1115/1.1640638

[12] J. Luo, K. R. Pattipati, L. Qiao, S. Chigusa, Model-Based Prognostic Techniques Applied to a Suspension System, *IEEE Transactions on Systems, Man, and Cybernetics - Part A: Systems and Humans*, Vol. 38, No. 5, pp. 1156-1168, September, 2008. https://doi.org/10.1109/TSMCA.2008.2001055

[13] M. Dong, D. He, A segmental hidden semi-Markov model (HSMM)-based diagnostics and prognostics framework and methodology, *Mechanical Systems and Signal Processing*, Vol. 21, No. 5, pp. 2248-2266, July, 2007. https://doi.org/10.1016/j.ymssp.2006.10.001

[14] PHM Society, PHM Society: PHM data challenge, May, 2010. https://phmsociety.org/phm_competition/2010-phm-society-conference-data-challenge/

[15] Pro-micron GmbH, Intelligent tool-holder - wear detection of every cutting edge with spike®, https://www.pro-micron.de/spike/?lang=en

[16] R.L. Graham, An efficient algorithm for determining the convex hull of a finite planar set, *Information Processing*

Letters, Vol. 1, No. 4, pp. 132-133, June, 1972.

[17] S. Zheng, K. Ristovski, A. Farahat, C. Gupta, Long Short-Term Memory Network for Remaining Useful Life estimation, *IEEE International Conference on Prognostics and Health Management*, Dallas, TX, USA, 2017, pp. 88-95.
https://doi.org/10.1109/ICPHM.2017.7998311

[18] J. Zhang, P. Wang, R. Yan, R. X. Gao, Long short-term memory for machine remaining life prediction, *Journal of Manufacturing Systems*, Vol. 48, Part C, pp. 78-86, July, 2018.
https://doi.org/10.1016/j.jmsy.2018.05.011

[19] T. Benkedjouh, K. Medjaher, N. Zerhouni, S. Rechak, Health assessment and life prediction of cutting tools based on support vector regression, *Journal of Intelligent Manufacturing*, Vol. 26, No. 2, pp. 213-223, April, 2015.
https://doi.org/10.1007/s10845-013-0774-6

Biographies

Der-Chen Huang received the BS degree in electronic engineering from Fung Chia University, Taiwan, in 1983, the MS degree in computer engineering from Florida Institute of Technology, U.S.A., in 1991, and the PhD degree in computer engineering from the Department of Computer Science and Information Engineering, Chung- Cheng University, Chiayi, Taiwan, R.O.C. in 2000. From 1983 to 1989, he worked as a design engineer with the Computer Communication Lab. (CCL)/Industrial Technology Research Institute (ITRI) and Chung-Shan Institute and Science of Technology (CSIST) when he was assigned to a partnership project at General Dynamics, Fort Worth, Texas, U.S.A. He was an associate professor with the Department of Electronic Engineering, National Chinyi Institute of Technology, Taichung, Taiwan, R.O.C. from 1991 to 2004. In 2004, he joined the Department of Computer Science and Engineering, National Chung Hsing University, Taichung, Taiwan, R.O.C. He was a director of Computer and Information Center of Chung Hsing University from 2007 to 2011. Currently, he is a professor of Chung Hsing University. Dr. Huang served as a reviewer for various technical journal and conferences and a member of editorial board of *Journal of Internet Technology*. He received the Best Paper Award from the 5th International Conference on Future Information Technology, Korea, in 2010. His research interests include VLSI design for testability and diagnosis, VLSI Digital Signal Process, Communication and Medical Image.

Yen-Ting Wu is currently pursuing a Ph.D. degree in Computer Science and Engineering at National Chung Hsing University, Taiwan. His research interests include machine learning techniques, networking, websites, and servers.

Yen-Hsiang Yang received his M.S. degree in Computer Science and Engineering from National Chung Hsing University, Taiwan, in 2021. His research interests include artificial intelligence and intelligent systems.

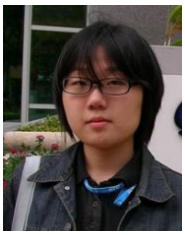

Ying-Yi Chu received her Ph.D. degree in Computer Science and Engineering from National Chung Hsing University, Taiwan, in 2018. She is currently an assistant professor in the Department of Electronic Engineering at National Kaohsiung Normal University. Her research interests include VLSI design, machine learning, and network.